The Use of Particle/Substrate Material Models in Simulation of Cold-Gas Dynamic-Spray Process

Saeed Rahmati and Abbas Ghaei

Cold spray is a coating deposition method in which the solid particles are accelerated to the substrate using a low temperature supersonic gas flow. Many numerical studies have been carried out in the literature in order to study this process in more depth. Despite the inability of Johnson-Cook plasticity model in prediction of material behavior at high strain rates, it is the model that has been frequently used in simulation of cold spray. Therefore, this research was devoted to compare the performance of different material models in the simulation of cold spray process. Six different material models, appropriate for high strain-rate plasticity, were employed in finite element simulation of cold spray process for copper. The results showed that the material model had a considerable effect on the predicted deformed shapes.

| Keywords	cold spray, high strain rate, simulation

1. Introduction

Cold spray is a coating deposition method in which the solid particles are accelerated to the substrate using a low temperature supersonic gas flow. In this process, unlike the thermal spray processes in which melted material is sprayed onto a surface, the particles are well below the melting point prior to impact on the substrate. In fact, the large kinetic energy of particles during impact causes an extreme and rapid plastic deformation and allows the particle to adhere to the surface. Experimental studies show that a successful bonding occurs only at velocities higher than a critical value which depends on the temperature and thermomechanical properties of the sprayed material (Ref 1). A schematic illustration of this process is shown in Fig. 1.

In general, it is very difficult to experimentally observe the deformation of particles during impact as the impact takes place in a very short time (tens of nanoseconds). Usually, the experimental studies only observe the deformed particles by microscopy. Therefore, numerical simulation of the cold spray process could be an effective way to study this process in more depth. Assadi et al. (Ref 1) utilized a numerical simulation of the process to study the bonding mechanism in cold spraying. Their analysis showed that the bonding mechanism was due to adiabatic shear instabilities which occur at the particle surface when the impact velocity is higher than or equal to the critical velocity. Grujicic et al. (Ref 2) also used finite element simulation to study the particles-substrate interactions during impact and reported that adiabatic shear instability and resultant plastic flow localization played a major role in the particle-substrate bonding. The actual bonding mechanism in cold spray process is still an open question. However, many experimental and computational results suggest that for a very short time during which particles and the substrate are in high temperature and high contact pressure, interfacial melting and inter-atomic diffusion do not have an important role in the particle/substrate bonding mechanism. High contact pressure, adiabatic shear instability, plastic localization that leads to jetting and clean contact surfaces are known as the necessary conditions for particle/substrate bonding. Once these conditions exist, bonding can occur via adhesion. However, high interfacial bonding strengths suggests that, in addition to adhesion, some type of nano/micro length-scale mechanical material mixing interlocking mechanism may also contribute to particle/substrate bonding (Ref 3). Schmit et al. (Ref 4) studied the coating quality through numerical simulation and experimental methods. In an effort to optimize the deposition process, Bae et al. (Ref 5) used finite element simulation to study the bonding features in the cold spray process. King et al. (Ref 6) also used experiment and numerical simulation to understand the effect of cold spray temperature and substrate hardness on particle deformation and adhesion. Kocimski et al. (Ref 7) analyzed the process using finite element modeling to explore the particle interactions with both substrate and neighboring particles. Li et al. (Ref 8, 9) also performed numerical simulation to find the effect of different numerical parameters on the accuracy of simulation results. Ghelichi et al. (Ref 10) developed a model for prediction of critical velocity and study the shear

Saeed Rahmati and **Abbas Ghaei**, Department of Mechanical Engineering, Isfahan University of Technology, 84156-83111 Isfahan, Iran. Contact e-mail: ghaei@cc.iut.ac.ir.
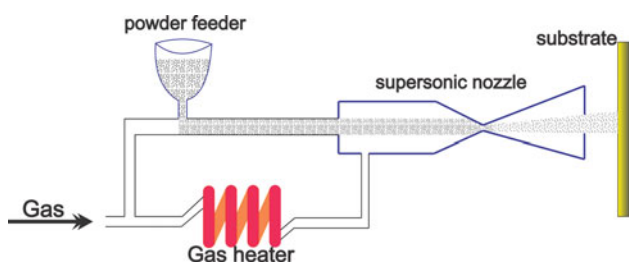
Fig. 1 Schematic illustration of cold spray process (Ref 1)
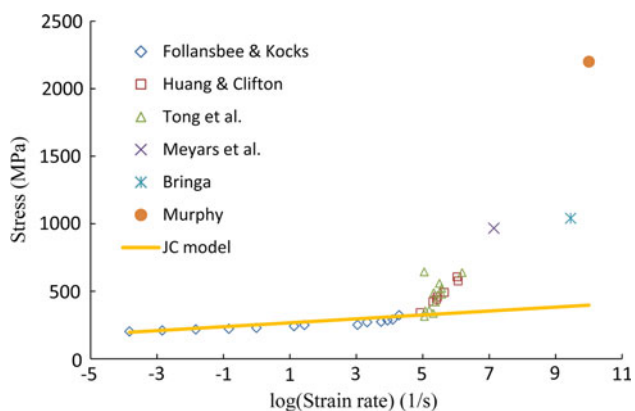
Fig. 2 The flow stress of copper at various strain rate (data taken from experiments (Ref 13-15, 17) and from molecular dynamics simulations (Ref 18) and prediction of Johnson-Cook model)

instability of the particle in the cold spray process. Recently, Moridi et al. (Ref 11) developed a new model for prediction of critical and erosion velocities. The model considers the porosity of particles and adhesion phenomenon in addition to the particle temperature and diameter.

For an accurate simulation of this process, it is necessary to predict the material behavior at extremely high strain rates. Up to now, several experimental tests have been proposed to determine the flow stress at high strain rates. The Hopkinson bar test was suggested by Hopkinson (Ref 12) as a one of the first methods to measure the stress pulse propagation in a metal bar. Later, Follansbee and Cocks (Ref 13) used Hopkinson bar test to obtain the flow stress for copper at strain rates between 10^{-4} s^{-1} to 10^{4} s^{-1}. Tong et al. (Ref 14) and Huang and Clifton (Ref 15) could further increase the strain rate to above 10^{6} s^{-1} using the pressure-shear technique. Later, Meyers et al. (Ref 16) could reach to 10^{7} s^{-1} using laser-induced shocks. Finally, Murphy et al. (Ref 17) used uniaxial shock compression test at 100 GPa to measure the shear stress at 10^{10} s^{-1} strain rate. In addition to experimental procedures, theoretical methods have also been developed to calculate the materials behavior at high strain rates. Bringa et al. (Ref 18) utilized the non-equilibrium molecular dynamics method to obtain the shear strength of copper at strain rates higher than 10^{9} s^{-1}. The results of

the above-mentioned studies have been summarized in Fig. 2 for pure copper. This figure shows that the behavior of copper changes dramatically at strain rates of around 10^{5} s^{-1}.

In addition to finding the experimental flow stress, a material model is also required in order to reproduce the material behavior in simulations. Johnson-Cook (JC) (Ref 19) hardening rule is the model frequently used in simulations of high strain rate problems in order to describe the dependency of materials behavior on strain rate and temperature. However, Gao and Zhang (Ref 20), Kim and Shin (Ref 21), and also Liang and Khan (Ref 22) indicated that the JC model exhibits acceptable results for copper only at strain rates of less than 10^{4} s^{-1}, as shown in Fig. 2. In other words, the JC model fails to accurately predict the material behavior when the slope of stress-strain rate changes abruptly. The common strain rates in cold spray are usually much higher than 10^{4} s^{-1}. Despite the inability of JC model in prediction of material behavior at high strain rates, it is the model that has been used in simulation of cold spray by almost all researchers (Ref 1, 2, 4-8, 10). Therefore, this research focuses on the importance of material model in simulation of cold spray process. To this end, several material models, appropriate for high strain rate plasticity, are employed in simulation of cold spray process for copper and the simulation results are compared with experiment. These models include Johnson and Cook (Ref 19), Modified Zerilli-Armstrong (MZA) (Ref 23), Voyiadjis-Abed (VA) (Ref 24), Preston-Tonk-Wallace (PTW) (Ref 25), Modified Khan-Huang-Liang (MKHL) (Ref 26), and Gao-Zhang (GZ) (Ref 20). Except the JC model, most of these models are not available as a built-in material model in today's commercial finite element packages, including ABAQUS. Thus, these models were implemented into ABAQUS/Explicit via VUHARD user subroutines and the cold spray process was simulated using this package. In order to make this study self-contained, these models are briefly introduced in the following section.

2. Models

2.1 JC model

This model was first introduced by Johnson and Cook (Ref 19). It was the first model that defined the flow stress as a function of plastic strain, strain rate, and temperature. After its introduction, the model became very famous because of its simplicity and ability to predict the flow stress fairly accurately in many practical situations. In this model, the flow stress is defined through:

$$\sigma = (A + B\varepsilon_{\mathrm{p}}^{n})(1 + C \ln \dot{\varepsilon}_{\mathrm{p}}^{*})(1 - T^{*m}) \qquad \text{(Eq 1)}$$

where A, B, n, C, and m are material constants, ε_{p} is the equivalent plastic strain, $\dot{\varepsilon}_{\mathrm{p}}^{*}$ is defined as $(\dot{\varepsilon}_{\mathrm{p}}/\dot{\varepsilon}_{0})$, $\dot{\varepsilon}_{\mathrm{p}}$ is the plastic strain rate, $\dot{\varepsilon}_{0}$ is the strain rate at which the material constants are obtained and is called the reference strain

Table 1 Parameters of JC model for copper (Ref 8)

A (MPa)	B (MPa)	C	m	n	T_r (K)	$\dot{\varepsilon}_0$ (1/s)
90	292	0.025	1.09	0.31	297	1

Table 2 Parameters of MZA model for copper (Ref 23)

c_2 (MPa)	c_4 (MPa)	$\dot{\varepsilon}_{p0}$ (1/s)	c_6 (MPa)
970	3.55×10^{-5}	1.76×10^8	50

Table 3 Parameters of VA model for copper (Ref 24)

β_1 (1/K)	β_2 (1/K)	Y_a (MPa)	B (MPa)	n	p	q
0.0006739	0.0000355	60	950	0.47	0.5	1.5

rate. Also, T^* is the homologous temperature and is defined as follows:

$$T^* = \begin{cases} 0 & \to T \prec T_r \\ \frac{T - T_r}{T_m - T_r} & \to T_r \prec T \prec T_m \\ 1 & \to T \succ T_m \end{cases} \quad \text{(Eq 2)}$$

where T_m is the melting temperature, T_r the reference or transition temperature, and T the absolute temperature. The JC model is only an empirical model and its parameters are usually obtained by fitting its response to the experimental response. It is clear from Eq 1 that the dependency of work hardening on the logarithm of strain rate is linear in this model which is very simple. For this reason, this model is not usually able to accurately predict the material behavior at very high strain rates. The JC model material parameters for copper are shown in Table 1. It is worth mentioning that the original JC model has been modified by Grujicic et al. (Ref 27) in order to improve its performance in analysis of hot metal working processes. The main reason for utilizing the original JC model in this study is that this is the model that has been frequently used in the simulation of cold spray process in the literature and the purpose of this study is to compare its performance with the other high strain rate plasticity models.

2.2 MZA Model

The initial ZA model is a physically based model proposed for materials that contain different types of crystals and their response is sensitive to strain rate and temperature. This model was proposed by Zerilli and Armstrong (Ref 28, 29). In this model, the flow stress is expressed by:

$$\sigma = A + \left[c_1 + c_2\sqrt{\varepsilon}\right]\exp[(-c_3 + c_4\ln\dot{\varepsilon})T] + c_5\varepsilon^n \quad \text{(Eq 3)}$$

where ε is the equivalent plastic strain, $\dot{\varepsilon}$ the plastic strain rate, T the temperature, and A, c_1, c_2, c_3, c_4, c_5 are all material constants. The exponential term in Eq 3 is used

to describe the thermal stress component based on experimental observation. This definition is inappropriate as the thermal stress component goes to zero only when the temperature tends to infinity. It is noted that, the thermal stress component must disappear at the melt temperature of material. In order to resolve this issue, it was modified by Abed et al. (Ref 23). The MZA model generally improves the results at temperatures above 300 K. However, the work hardening is expressed independent of temperature and strain rate just like the initial ZA model. This is why these models are not appropriate to model the materials whose responses strongly depend on temperature and strain rate.

The flow stress in MZA model is given by:

$$\sigma = c_2\varepsilon_p^{0.5}\left(1 - X^{1/2} - X + X^{3/2}\right) + c_6 \quad \text{(Eq 4)}$$

where $X = c_4 T \ln\left(1/\dot{\varepsilon}_p^*\right)$, $\dot{\varepsilon}_p^* = \dot{\varepsilon}_p/\dot{\varepsilon}_{p0}$, $\dot{\varepsilon}_p$ is the plastic strain rate, $\dot{\varepsilon}_{p0}$ the reference plastic strain rate, ε_p the plastic strain, and c_2, c_4, c_6 are all material constants. The MZA model material parameters for copper are shown in Table 2.

2.3 VA Model

After the introduction of the ZA model, a lot of efforts were made to propose new models with the purpose of improving the prediction of material behavior at high temperature and strain rates. Among these, Voyiadjis and Abed (Ref 24) presented a new hardening law based on the ZA model. This model could improve the prediction of material behavior at high temperatures and strain rates compared to the ZA model. The VA model is defined as follows:

$$\sigma = B\varepsilon_p^n(1 - (\beta_1 T - \beta_2 T \ln\dot{\varepsilon}_p)^{1/q})^{1/p} + Y_a \quad \text{(Eq 5)}$$

where ε_p is the equivalent plastic strain, $\dot{\varepsilon}_p$ the plastic strain rate, T the temperature, and B, β_1, β_2, Y_a, p, q, and n are all material constants. Table 3 lists the VA model material parameters for copper.

2.4 PTW Model

This model was developed by Preston et al. (Ref 25) to describe the behavior of materials at very high strain rates. It is a complex constitutive model proposed based on the dislocation motion during plastic deformation. The model is written as follows:

$$\sigma = 2\left[\tau_s + \alpha\ln\left[1 - \varphi\exp(-\beta - \frac{\theta\varepsilon_p}{\alpha\varphi})\right]\right]\mu(p, T) \quad \text{(Eq 6)}$$

$$\alpha = \frac{s_0 - \tau_y}{d}, \; \beta = \frac{\tau_s - \tau_y}{\alpha}, \; \varphi = \exp(\beta) - 1 \quad \text{(Eq 7)}$$

where ε_p is the plastic strain, τ_s the normalized work hardening saturation stress, τ_y the normalized yield stress, θ the hardening constant, d a dimensionless material constant, and s_0 the value of τ_s at zero temperature.

Table 4 Parameters of PTW model for copper (Ref 25)

s_0	s_∞	y_0	y_∞	d	k	γ	θ	M (amu)	s_1	y_1	y_2
0.0085	0.00055	0.0001	0.0001	2	0.11	0.00001	0.025	63.546	0.25	0.094	0.575

Table 5 Parameters of MKHL model for copper (Ref 37)

A (MPa)	B (MPa)	n_1	n_0	C	p	m
317	123	−0.132	0.543	1.81×10^{-4}	2.641	6.500

Moreover, μ denotes the shear modulus and is assumed to be a function of temperature and density of the material. τ_s and τ_y are defined as:

$$\begin{cases} \tau_s = \max\left\{ s_0 - (s_0 - s_\infty)\text{erf}\left[k\hat{T}\ln\left(\frac{\gamma\dot{\zeta}}{\dot{\varepsilon}_p}\right)\right], s_0\left(\frac{\dot{\varepsilon}_p}{\gamma\dot{\zeta}}\right) \right\} \\ \tau_y = \max\left\{ y_0 - (y_0 - y_\infty)\text{erf}\left[k\hat{T}\ln\left(\frac{\gamma\dot{\zeta}}{\dot{\varepsilon}_p}\right)\right], \min\left\{ y_1\left(\frac{\dot{\varepsilon}_p}{\gamma\dot{\zeta}}\right), s_0\left(\frac{\dot{\varepsilon}_p}{\gamma\dot{\zeta}}\right) \right\} \right\} \end{cases} \quad \text{(Eq 8)}$$

where $\hat{T} = T/T_m$, T is the temperature, T_m the melting temperature, s_∞ the value of τ_s near the melt temperature, y_0 and y_∞ the values of τ_y at zero and at very high temperature, respectively. Furthermore, γ, k, s_1, y_1, and y_2 are all material parameters and

$$\dot{\zeta} = \frac{1}{2}\left(\frac{4\pi\rho}{3M}\right)^{1/3}\left(\frac{\mu(\rho,T)}{\rho}\right)^{1/2} \quad \text{(Eq 9)}$$

where ρ is the density and M denotes the atomic mass. The PTW model material parameters for copper are shown in Table 4.

2.5 MKHL Model

The primary Khan-Huang-Liang (KHL) model was presented by Khan and Liang (Ref 30, 31). They modified the JC model by considering the work hardening as a coupled function of strain and strain rate. Later, Huh et al. (Ref 26, 32) presented the modified version of KHL model. This model correlates better to the experimental results in compression with the KHL model. In this model, the flow stress is given by:

$$\sigma = \left(A + B\left(1 - \frac{\ln\dot{\varepsilon}}{\ln D_0^p}\right)^{n_1}\varepsilon^{n_0}\right)(1 + C(\ln\dot{\varepsilon}^*)^p)(1 - T^{*m}) \quad \text{(Eq 10)}$$

where A, B, C, n_0, n_1, p, and m are all material constants. Furthermore, T^* is defined in Eq (2) and D_0^p is chosen to be 10^9 s^{-1}. The MKHL model material parameters for copper are shown in Table 5.

2.6 GZ Model

This model was proposed by Gao and Zhang (Ref 20) for deformation of materials at strain rates of higher than 10^4 s^{-1}. According to them, the previous models did not have the ability to predict the correct behavior of copper at strain rates above 10^4 s^{-1}. Unlike the other models, the density of dislocations is not assumed to be constant in this model. In fact, it is defined as a function of equivalent plastic strain, strain rate and temperature. The flow stress is defined by:

$$\sigma = \sigma_{th} + \sigma_{ath} \quad \text{(Eq 11)}$$

where σ_{th} and σ_{ath} are thermal and non-thermal stress components, respectively.

The thermal stress component is written as follows:

$$\sigma_{th} = \hat{C}.\sqrt{1 - \exp\left[-k_0\left(\frac{\dot{\varepsilon}}{\dot{\varepsilon}_{s0}}\right)^{-c_1 T}\varepsilon\right]}$$
$$\cdot\sqrt{\left\{1 + \tanh\left[c_0\log\left(\frac{\dot{\varepsilon}}{\dot{\varepsilon}_{s0}}\right)\right]\right\}\cdot\left(\frac{\dot{\varepsilon}}{\dot{\varepsilon}_{s0}}\right)^{c_1 T}}$$
$$\cdot\left\{1 - \left[-c_2 T\ln\left(\frac{\dot{\varepsilon}}{\dot{\varepsilon}_0}\right)\right]^{1/q}\right\}^{1/p} \quad \text{(Eq 12)}$$

where $\hat{C}$ is reference thermal stress, k_0, c_0, c_1, c_2, p, and q are all material constants for thermal stress component. Moreover, ε and $\dot{\varepsilon}$ are equivalent plastic strain and equivalent plastic strain rate, respectively, and $\dot{\varepsilon}_0$ and $\dot{\varepsilon}_{s0}$ are reference strain rate and saturated strain rate, respectively.

The non-thermal stress component is expressed by:

Table 6 Parameters of GZ model for copper (Ref 20)

Parameters of Eq 11-13							Parameters of Eq 14				
$\bar{C}$ (MPa)	k_0	c_0	c_1 (1/K)	c_2 (1/K)	p	q	$\bar{C}$ (MPa)	k_0	c_2 (1/K)	p	q
9850	10	0.483	4.93×10^{-5}	1×10^{-4}	0.45	1	959	0.82	5.75×10^{-5}	0.91	1.47
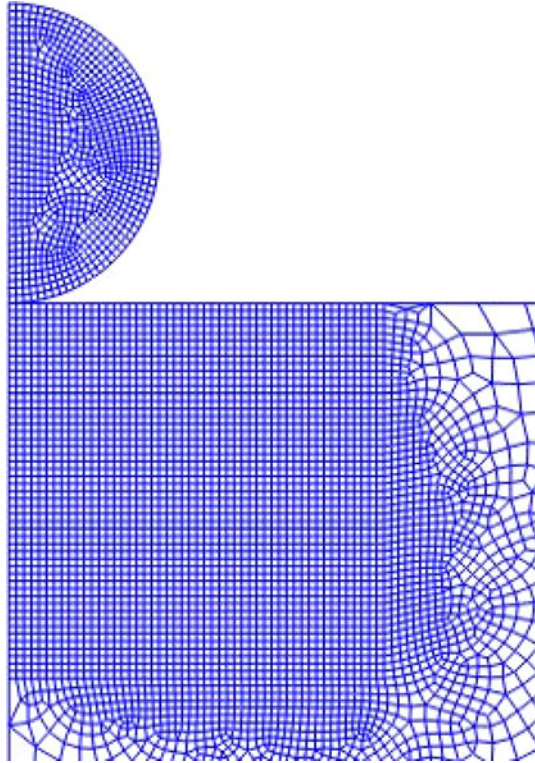
Fig. 3 The finite element model of the cold spray process

$$\sigma_{ath} = \sigma_G + B[1 - \exp(-k_{a0}\varepsilon)]^{1/2} \qquad \text{(Eq 13)}$$

where σ_G is the stress due to initial defects, B and k_{a0} are material constants for non-thermal stress component. Table 6 lists the GZ model material parameters for copper.

Gao and Zhang have also presented a unified model for strain rates less than 10^4 s^{-1} which is defined as follows:

$$\sigma = \sigma_G + \hat{C} \cdot \sqrt{1 - \exp(-k_0\varepsilon)} \cdot \left\{ 1 - \left[-c_2 T \ln\left(\frac{\dot{\varepsilon}}{\dot{\varepsilon}_0}\right) \right]^{1/q} \right\}^{1/p}.$$
$$\text{(Eq 14)}$$

3. Finite Element Model

The impacting behavior of a particle on a substrate was simulated using ABAQUS/explicit. Assuming that the particle is a perfect sphere, an axisymmetric model can be built to model the process, as shown in Fig. 3. Therefore,

Table 7 Properties of copper used in simulations (Ref 8, 38, 39)

Density (kg/m^3)	8,960
Thermal conductivity (W/(m.K))	386
Specific heat (J/(kg.K))	383
Shear modulus (GPa)	45
EOS parameters: C_0 (m/s), s, Γ_0	3933000, 1.5, 1.99
Reference temperature (K)	297
Melting point (K)	1,356
Inelastic heat fraction	0.9

the substrate geometry is assumed to be a cylinder whose radius and height are five times larger than the particle radius. It should also be pointed out that simulations results showed no sensitivity to larger dimensions of the cylinder. The particle diameter is 20 microns. As for the particle-substrate interaction, a surface to surface contact was defined and the coefficient of friction was assumed to be 0.4 (Ref 8).

As the properties of copper are suitable for the cold spray process, it has been widely studied by many researchers (Ref 1, 2, 4, 8-10). In this study, both the particle and substrate are assumed to be pure copper with the properties shown in Table 7. The initial temperature (T_0) and the initial velocity of particle (V_p) were assumed to be 297 K and 500 m/s, respectively.

The elastic response of the material was assumed to follow a linear Mie-Gruneision equation of state (EOS) instead linear elasticity model, because the linear elasticity model is adequate for low and moderate particle impact velocities (Ref 1). The EOS model has the following form (Ref 33):

$$p - p_H = \rho\Gamma(E_m - E_H) \qquad \text{(Eq 15)}$$

where p_H and E_H are the Hugoniot pressure and specific energy, respectively, Γ is the Gruniesen ratio, ρ is the current density, and E_m is the specific energy (the internal energy per unit mass). Equation 15 shows that EOS defines only the material's hydrostatic behavior. In order to define the deviatoric behavior, the deviatoric response was assumed to be governed by the linear elastic model with shear modulus of 45 GPa.

4. Results

Due to the high velocity of particle during impact, both the particle and substrate start to deform at a very high strain rate. The temperature also starts to increase due to

friction and dissipative mechanisms in the material. Therefore, the flow stress is influenced by two factors that act in opposite directions. The first factor is the work hardening that occurs due to dislocation movement and dislocation generation within the crystalline structure of the material (Ref 34). So, the work hardening increases the flow stress as the plastic deformation is accumulated. The second factor is the softening of material due to temperature rise, i.e., thermal softening. Therefore, for an accurate simulation of cold spray process, not only the dependency of flow stress on strain rate should be accurately modeled, but also the work hardening and thermal softening phenomena must be accurately described. Because it is very difficult, if possible, to experimentally measure the flow stress during deformation in the cold spray process, the deformed shape of the particle is used in this study as a measure of the accuracy of flow stress prediction. The amount of particle penetration into substrate, the height of deformed particle and the jetting of material are among the important factors that can be used to compare the predicted and experimental deformed shapes. It is noted that an accurate prediction of flow stress is an essential key factor in an accurate prediction of the deformed shape.
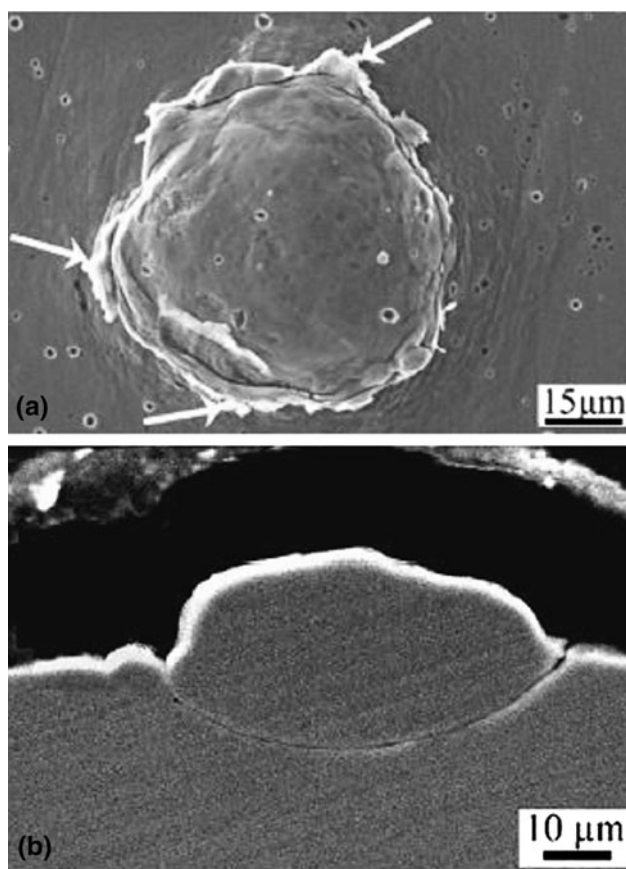
Fig. 4 The deposited copper particle on polished copper substrate: (a) surface, (b) cross-section morphologies at velocity of 500 m/s (Ref 35)

Figure 4 shows the micrograph of a copper particle sprayed on a copper substrate at a velocity of 500 m/s (Ref 35). In order to observe the depth of particle penetration into the substrate, the cross-section of the figure has also been shown in Fig. 4b.

In the cold spray process, a small amount of material jetting is usually observed as marked by arrows in Fig. 4a. The temperature considerably rises near the contact zone due to conversion of friction and plastic works into heat. This temperature rise results in more thermal softening of the material in that area. Therefore, a larger deformation occurs in the contact zone known as jetting. The occurrence of jetting has also been attributed to the localized deformation in the contact zone under dynamic loading (Ref 7) and even possible melting of material (Ref 4).

Figure 5 compare the final deformed shape of the particle obtained by experiment and simulation using different material models. The cross-section view of experimental deformed shape, as shown in Fig. 4b and 5, indicates that the deformation is not totally symmetric about the vertical axis. However, because it was assumed that the material was isotropic and the initial geometry of the particle was a sphere, the finite element simulation will always predict a symmetric deformed shape in this study. Figure 5 shows that the JC model overpredicts the deformation of both particle and substrate. This is in contrast to the GZ model prediction where the deformation is underestimated for both substrate and particle, as shown in Fig. 5. In addition, the JC model predicts a large amount of jetting, while the GZ model does not predict the material jetting at all. Therefore, these observations suggest that the JC model underestimates the flow stress, while the GZ model overestimates the flow stress. Figure 5 shows that the VA model predicts the particle penetration and deformation fairly accurately. However, no jetting is observed in the prediction by this model. The amount of penetration, particle deformation and jetting are all predicted fairly well by the PTW model, as shown in Fig. 5. The MZA model predicts the penetration and particle deformation almost accurately, as shown in Fig. 5. However, the jetting phenomenon is neglected by this model. Finally, the predicted deformed shape by MKHL is relatively in good agreement with experiment, as shown in Fig. 5.

In order to quantify the error between the simulation and experiment, the following error functions are defined:

$$\delta_1 = \left| \frac{D_E - D_m}{D_E} \right| \times 100 \qquad (\text{Eq } 16)$$
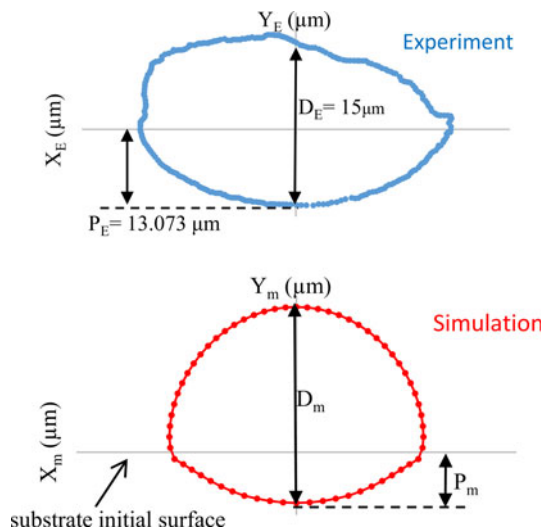
$$\delta_2 = \left| \frac{P_E - P_m}{P_E} \right| \times 100 \qquad (\text{Eq } 17)$$

$$\delta_3 = \frac{1}{n} \sum_{i=1}^{n} |y_{Ei} - y_{mi}| \qquad (\text{Eq } 18)$$

where D_E, D_m, P_E, and P_m have been defined in Fig. 6. Moreover, δ_1 and δ_2 are the percentage of relative errors in prediction of particle deformation error (D_E) and penetration error (P_E), respectively. In addition, δ_3 is the
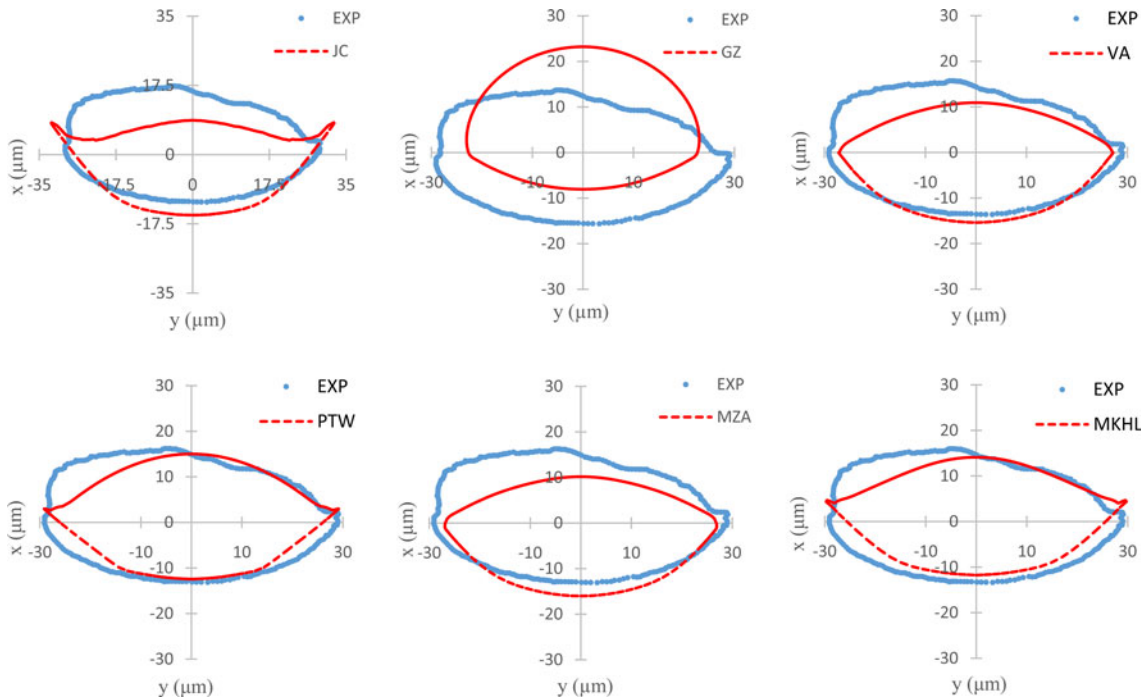
Fig. 5 Final deformed shape of the particle

Fig. 6 The definition of parameters P_E, P_m, D_E, and D_m

mean absolute error, n the number of nodes located in the circumference of the particle in the finite element model, y_E the y coordinate of nodes after deformation for experimental data and y_m the y coordinate of nodes after deformation for predicted data. The errors δ_1, δ_2, and δ_3 associated with each model were calculated using Eqs 16-18 and plotted in Fig. 7a-c. The figures show that the particle deformation is best predicted by the PTW model. The PTW model also predicts the particle penetration relatively accurately. As shown in Fig. 7c, the total error criterion, δ_3, shows that the PTW model generally results in the smallest amount of error. The figure also shows that
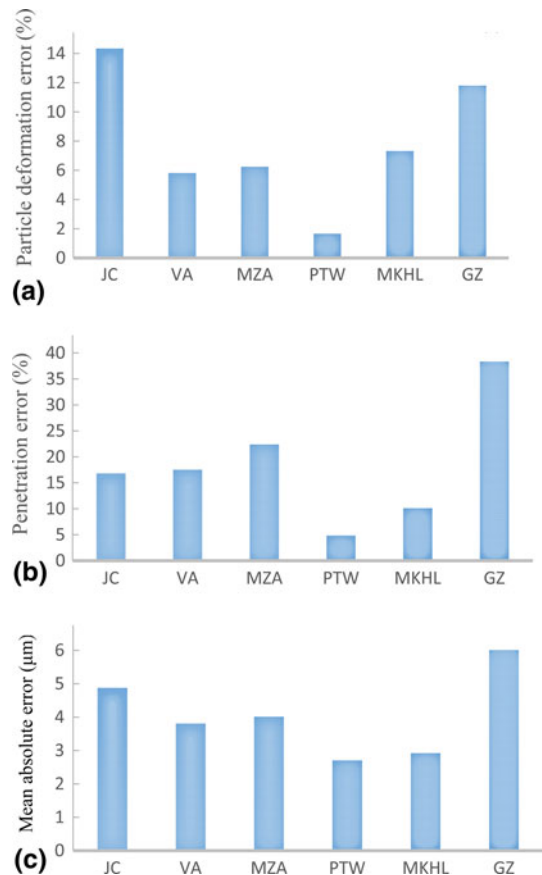
Fig. 7 The errors associated with each model: (a) particle deformation error, (b) penetration error, (c) mean absolute error
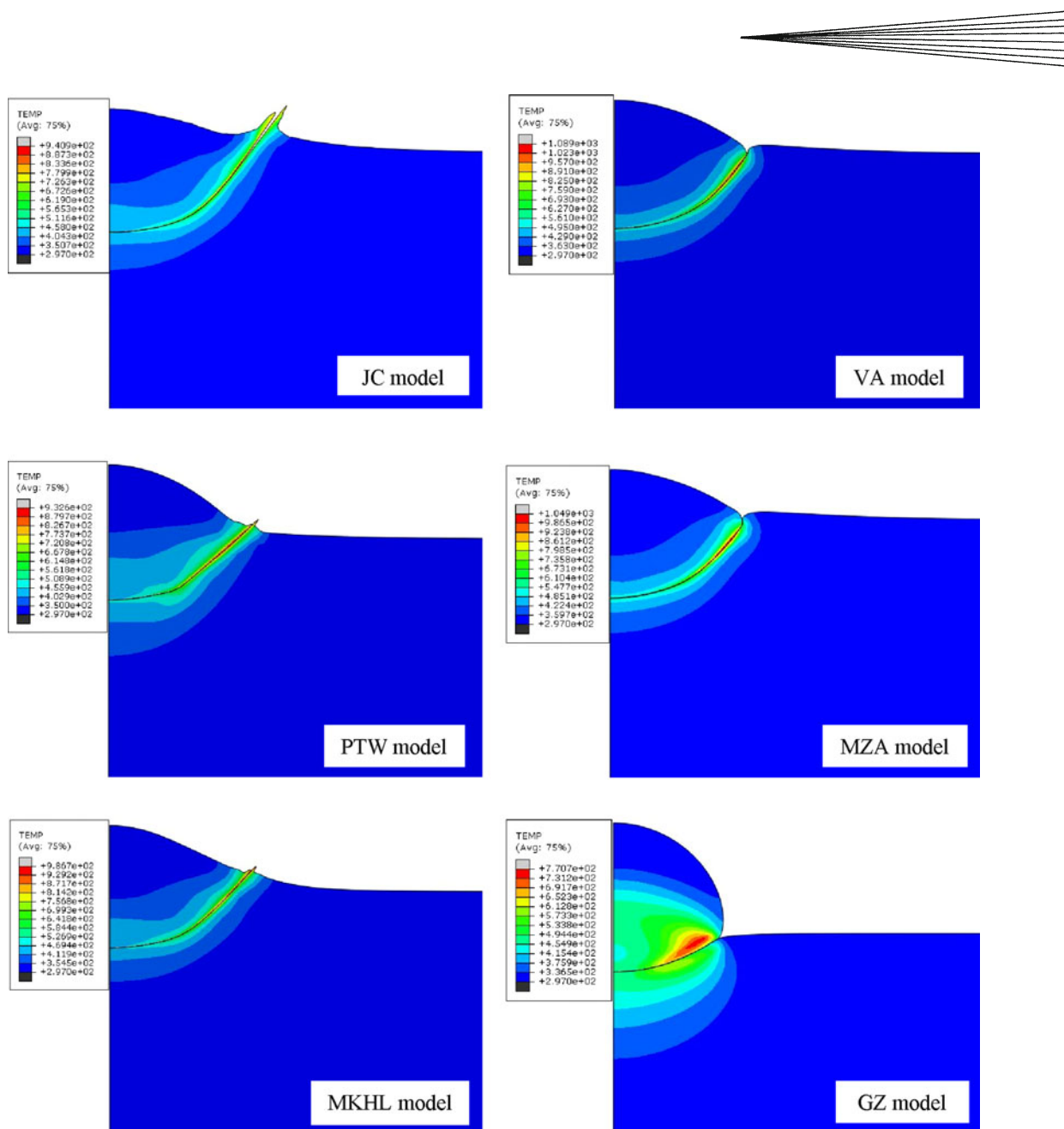
**Fig. 8** Temperature distribution in terms of Kelvin at the end of deformation

the total error associated with the MKHL model is relatively small.

Figure 8 shows the contour of temperature distribution predicted by each model. The maximum and minimum temperature rises are predicted by the VA and JC models, respectively. The maximum temperature rise in all simulations takes place at the particle-substrate interface where the jetting phenomenon is expected to occur. The largest and smallest temperature rises are predicted by the VA and GZ models, respectively.

Figure 9 shows the history of strain rate for an element at the copper particle surface during the particle impact. These figures show that the strain rate changes from zero to more than $1 \times 10^8 \text{ s}^{-1}$. Therefore, the material model needs to accurately predict the flow stress within this

range. Figure 10 compares the flow stress predicted by each model with that of the experiment at a constant strain of 0.15. The figures show that only the PTW model can accurately predict the flow stress at a wide strain rate ranges. The GZ model overpredicts the flow stress at high strain rates, a conclusion already drawn from the predicted deformed shape by this model. The rest of the models underestimate the flow stress at high strain rate, i.e., above 10^6 s^{-1}. It should be emphasized that these comparisons are made at a particular strain, i.e., 15%. As the plastic strain is accumulated, the predicted work hardening usually increases the predicted flow stress. If this increase is overestimated, the predicted flow stress may improve due to counterbalancing errors. In order to study this in more depth, the stress-strain curves predicted
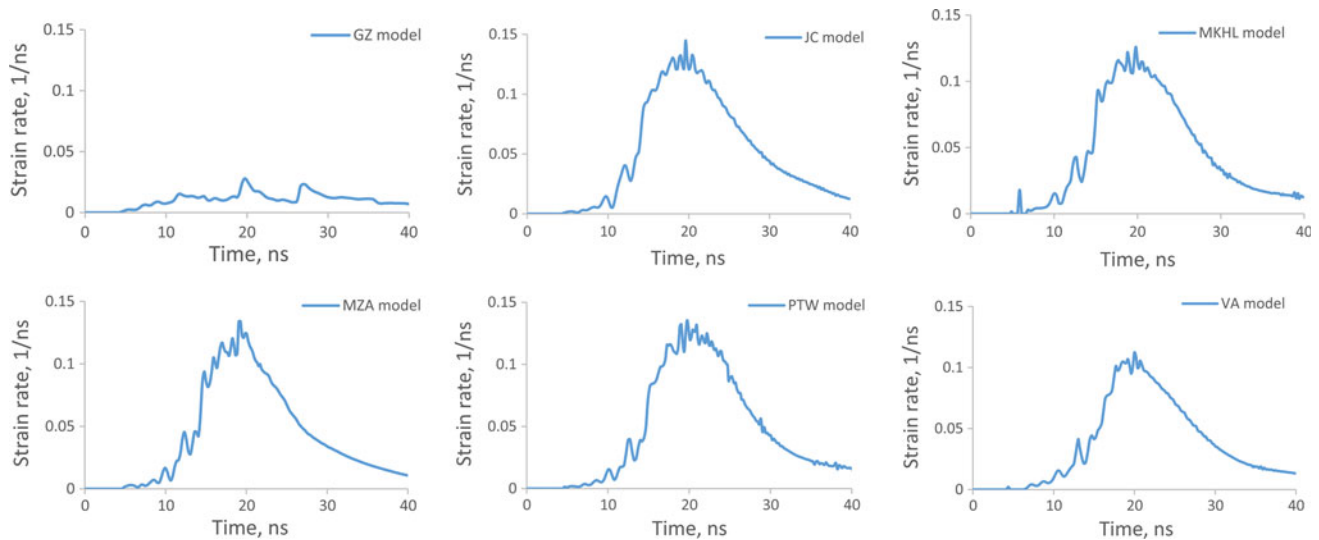
Fig. 9 The strain rate history for an element at the particle-substrate interface during impact
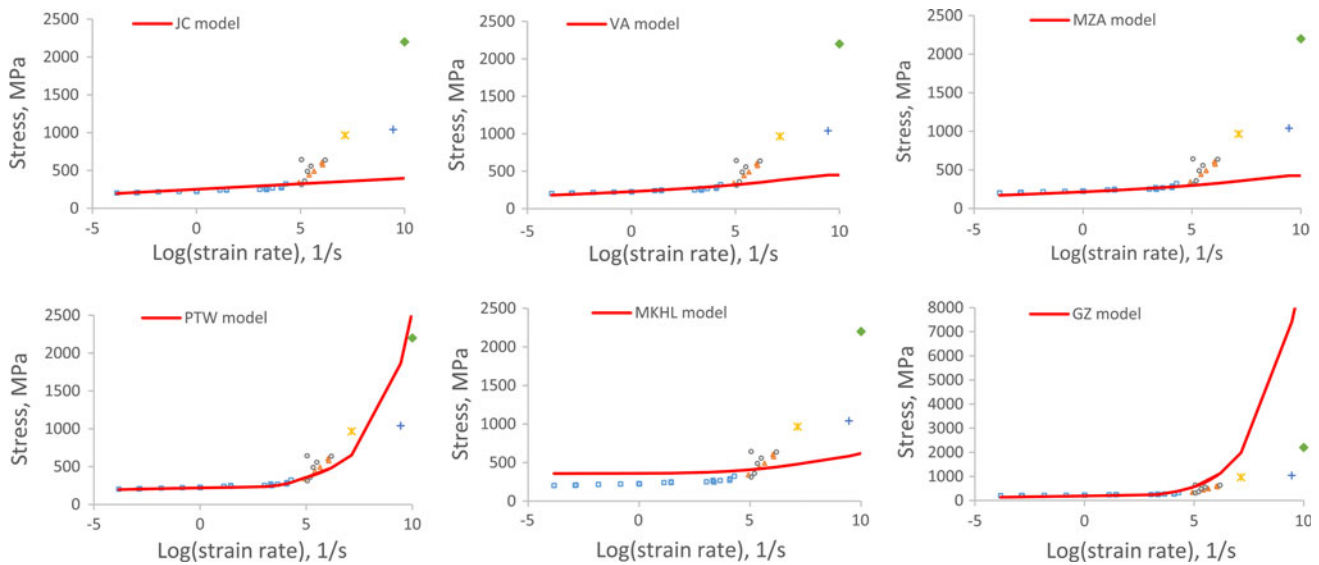

**Fig. 10** The flow stress for copper at various strain rates

by each model are compared with the experimental results obtained by Rittel et al. (Ref 36) at strain rate of 32,000 s⁻¹. As shown in Fig. 11, the flow stress is over-predicted at large strains by some models, e.g., VA model. This figure together with Fig. 10 indicates that counter-balancing of errors is possible as the accumulated plastic strain in this process is quite large as shown in Fig. 12. Therefore, it is generally difficult to predict whether the particle deformation in cold spray should be overesti-mated or underestimated by these models, i.e. VA, MZA, and GZ models. In fact, the cold spray process parameters determine the accuracy of simulations by these models. However, it is also interesting to look at the flow stress predicted by JC model. This model underestimates the flow stress at both different strain rates and different strains, as shown in Fig. 10 and 11. Therefore, one may

expect that this model always overpredicts the deforma-tion in the cold spray process. As shown in Fig. 6, this model does overpredict the deformation in the simulation of cold spray process. Finally, the PTW model predicts the flow stress relatively accurately within a broad range of strains and strain rates, as shown in Fig. 10 and 11. Therefore, this model is able to simulate the cold spray process relatively accurately.

In order to compare the performance of the hardening models in prediction of the critical velocity, the method developed by Moridi et al. (Ref 11) is used to predict the critical velocity. The porosity of particle was assumed to be zero. According to the literature, the critical velocity for a 40-μm diameter copper particle is about 450 to 500 m/s (Ref 9). Figure 13 compares the critical velocities predicted by various models. It can be seen that the critical
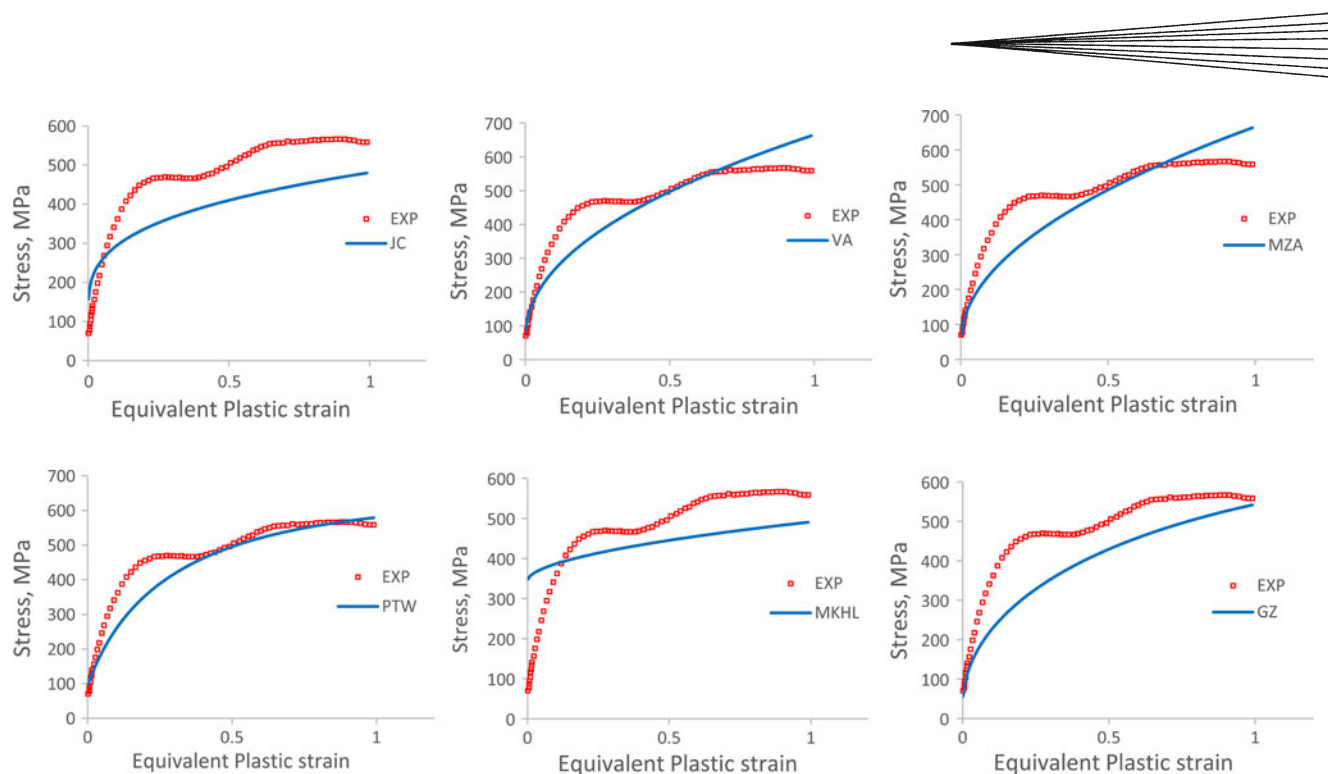
Fig. 11 Compression between the experimental (Ref 36) and predicted flow stress at strain rate of 3,200 s^{-1}
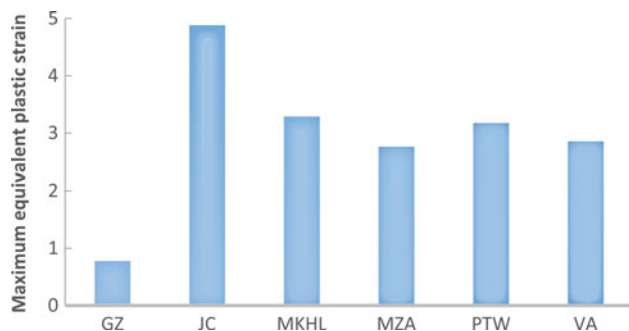
Fig. 12 Maximum equivalent plastic strain that is predicted by various models
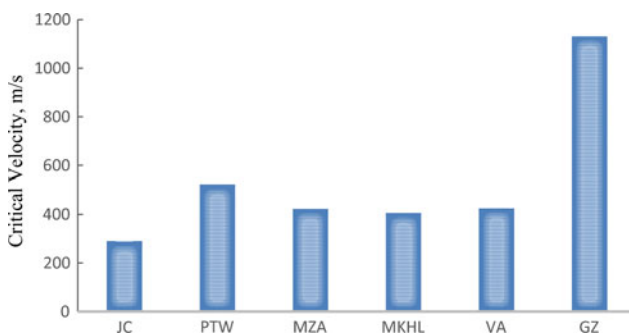
Fig. 13 The prediction of critical velocities using different material models and comparison with experimental data

velocity is predicted fairly accurately by the PTW model. The error associated with JC and GZ models is quite large compared to the other models. Furthermore, the predicted

critical velocity by MZA, MKHL, and VA models is also in good agreement with experiment.

5. Conclusion

The cold spray process was simulated for pure copper using six different material models appropriate for high strain rate plasticity. The predicted deformed shapes by each model were then compared with that of the experiment. The conclusions of this study can be summarized as follows:

a. The JC model underestimates the flow stress at very high strain rates and, therefore, overpredicts the particle deformation in the cold spray process. Thus, this model is not generally appropriate for simulation of cold spray process.

b. In general, the GZ overestimates the flow stress for copper and cannot accurately predict the deformed shape in the cold spray process.

c. The jetting phenomenon is captured by JC, PTW, and MKHL models. However, it was not observed in simulations using the MZA, VA, and GZ models.

d. The VA, MKHL, and MZA models do not predict the flow stress over a wide range of strains and strain rates. Thus, the cold spray process may not be simulated accurately by these models. In fact, the cold spray process parameters that determine the history of strain and strain rate during the deformation determines the accuracy of cold spray simulation by these models.

e. The PTW model predicts the deformation in the cold spray process fairly accurately.

f. Among the six models used in this study, only the PTW, MZA, MKHL, and VA models predict the critical velocity fairly accurately.

References

1. H. Assadi, F. Gärtner, T. Stoltenhoff, and H. Kreye, Bonding Mechanism in Cold Gas Spraying, *Acta Mater.*, 2003, **51**(15), p 4379-4394

2. M. Grujicic, C.L. Zhao, W.S. DeRosset, and D. Helfritch, Adiabatic Shear Instability Based Mechanism for Particles/Substrate Bonding in the Cold-Gas Dynamic-Spray Process, *Mater. Des.*, 2004, **25**(8), p 681-688

3. M. Grujicic, J.R. Saylor, D.E. Beasley, W.S. DeRosset, and D. Helfritch, Computational Analysis of the Interfacial Bonding Between Feed-Powder Particles and the Substrate in the Cold-Gas Dynamic-Spray Process, *Appl. Surf. Sci.*, 2003, **219**(3-4), p 211-227

4. T. Schmidt, F. Gärtner, H. Assadi, and H. Kreye, Development of a Generalized Parameter Window for Cold Spray Deposition, *Acta Mater.*, 2006, **54**(3), p 729-742

5. G. Bae, S. Kumar, S. Yoon, K. Kang, H. Na, H.-J. Kim, and C. Lee, Bonding Features and Associated Mechanisms in Kinetic Sprayed Titanium Coatings, *Acta Mater.*, 2009, **57**(19), p 5654-5666

6. P.C. King, G. Bae, S.H. Zahiri, M. Jahedi, and C. Lee, An Experimental and Finite Element Study of Cold Spray Copper Impact onto Two Aluminum Substrates, *J. Thermal Spray Technol.*, 2010, **19**(3), p 620-634

7. J. Kocimski, R.G. Maev, and V. Leshchynsky, Modeling of Particle Consolidation by Cold Spray, International Thermal Spray Conference & Exposition 2010, Thermal Spray: Global Solutions for Future Application. DVS-ASM, Materials Park, 2010, p. 774-779

8. W.Y. Li, C. Zhang, C.-J. Li, and H. Liao, Modeling Aspects of High Velocity Impact of Particles in Cold Spraying by Explicit Finite Element Analysis, *ASM Int.*, 2009, **18**, p 921-933

9. W.-Y. Li, S. Yin, and X.-F. Wang, Numerical Investigations of the Effect of Oblique Impact on Particle Deformation in Cold Spraying by the SPH Method, *Appl. Surf. Sci.*, 2010, **256**(12), p 3725-3734

10. R. Ghelichi, S. Bagherifard, M. Guagliano, and M. Verani, Numerical Simulation of Cold Spray Coating, *Surf. Coat. Technol.*, 2011, **205**(23-24), p 5294-5301

11. A. Moridi, S. Hassani-Gangaraj, and M. Guagliano, A Hybrid Approach to Determine Critical and Erosion Velocities in the Cold Spray Process, *Appl. Surf. Sci.*, 2013, **273**, p 617-624

12. B. Hopkinson, A Method of Measuring the Pressure Produced in the Detonation of High Explosives or by the Impact of Bullets, *Proc. R. Soc. Lond. Ser. A*, 1914, **89**(612), p 411-413

13. P.S. Follansbee and U.F. Kocks, A Constitutive Description of the Deformation of Copper Based on the Use of the Mechanical Threshold Stress as an Internal State Variable, *Acta Mater.*, 1987, **36**, p 81-93

14. W. Tong and R.J. Clifton, Pressure-Shear Impact Investigation of Strain Rate History Effects in Oxygen-Free High-Conductivity Copper, *Mech. Phys. Solids*, 1991, **40**, p 1251-1294

15. S. Huang, and R.J. Clifton, Macro and Micro-Mechanics of High Velocity Deformation and Fracture, IUTAM Symposium on MMMHVDF, Tokyo, 1985, p. 63

16. M.A. Meyers, F. Gregori, B.K. Kad, M.S. Schneider, D.H. Kalantar, B.A. Remington, G. Ravichandran, T. Boehly, and J.S. Wark, Laser-Induced Shock Compression of Monocrystalline Copper: Characterization and Analysis, *Acta Mater.*, 2003, **51**(5), p 1211-1228

17. W.J. Murphy, A. Higginbotham, G. Kimminau, B. Barbrel, E.M. Bringa, J. Hawreliak, R. Kodama, M. Koenig, W. McBarron, M.A. Meyers, B. Nagler, N. Ozaki, N. Park, B. Remington, S.

18. Rothman, S.M. Vinko, T. Whitcher, and J.S. Wark, The Strength of Single Crystal Copper Under Uniaxial Shock Compression at 100 GPa, *J. Phys.*, 2010, **22**, p 1-6

18. E.M. Bringa, K. Rosolankova, R.E. Rudd, B.A. Remington, J.S. Wark, M. Duchaineau, D.H. Kalantar, J. Hawreliak, and J. Belak, Shock Deformation of Face-Centred-Cubic Metals on Subnanosecond Timescales, *Nat. Mater.*, 2006, **5**(10), p 805-809

19. G.R. Johnson and W.H. Cook, Fracture Characteristics of Three Metals Subjected to Various Strains, Strain Rates, Temperatures and Pressures, *Eng. Fract. Mech.*, 1985, **21**(1), p 31-48

20. C.Y. Gao and L.C. Zhang, Constitutive Modelling of Plasticity of fcc Metals Under Extremely High Strain Rates, *Int. J. Plast.*, 2012, **32-33**, p 121-133

21. J.-B. Kim and H. Shin, Comparison of Plasticity Models for Tantalum and a Modification of the PTW Model for Wide Ranges of Strain, Strain Rate, and Temperature, *Int. J. Impact Eng.*, 2009, **36**(5), p 746-753

22. R. Liang and A.S. Khan, A Critical Review of Experimental Results and Constitutive Models for BCC and FCC Metals Over a Wide Range of Strain Rates and Temperatures, *Int. J. Plast.*, 1999, **15**, p 963-980

23. F.H. Abed, G.Z. Voyiadjis, B. Rouge, and Louisiana, A Consistent Modified Zerilli-Armstrong Flow Stress Model for BCC and FCC Metals for Elevated Temperatures, *Acta Mech.*, 2005, **175**, p 1-18

24. G.Z. Voyiadjis and F.H. Abed, Microstructural Based Models for bcc and fcc Metals with Temperature and Strain Rate Dependency, *Mech. Mater.*, 2003, **37**, p 355-378

25. D.L. Preston, D.L. Tonks, and D.C. Wallace, Model of Plastic Deformation for Extreme Loading Conditions, *Appl. Phys.*, 2003, **93**, p 211-220

26. H. Huh, H. Lee, and J. Song, Dynamic Hardening Equation of the Auto-Body Steel Sheet with the Variation of Temperature, *Int. J. Automot. Technol.*, 2012, **13**(1), p 43-60

27. M. Grujicic, B. Pandurangan, C.F. Yen, and B. Cheeseman, Modifications in the AA5083 Johnson-Cook Material Model for Use in Friction Stir Welding Computational Analyses, *J. Mater. Eng. Perform.*, 2012, **21**(11), p 2207-2217

28. R. Armstrong and F. Zerilli, Dislocation Mechanics Aspects of Plastic Instability and Shear Banding, *Mech. Mater.*, 1994, **17**(2), p 319-327

29. F.J. Zerilli and R.W. Armstrong, Dislocation Mechanics Based Constitutive Relations for Material Dynamics Calculations, *J. Appl. Phys.*, 1987, **61**(5), p 1816-1825

30. A.S. Khan and R. Liang, Behaviors of Three BCC Metal Over a Wide Range of Strain Rates and Temperatures: Experiments and Modeling, *Int. J. Plast.*, 1999, **15**(10), p 1089-1109

31. A.S. Khan and R. Liang, Behaviors of Three BCC Metals During Non-proportional Multi-axial Loadings: Experiments and Modeling, *Int. J. Plast.*, 2000, **16**(12), p 1443-1458

32. H. Huh, J.H. Song, and H.J. Lee, Dynamic Tensile Tests of Auto-Body Steel Sheets with the Variation of Temperature, *Solid State Phenom.*, 2006, **116**, p 259-262

33. D. Simulia, ABAQUS 6.11 Analysis User's Manual, *Abaqus 6.11 Documentation*, 2011, p 22.22

34. E.P. De Garmo, J.T. Black, and R.A. Kohser, *DeGarmo's Materials and Processes in Manufacturing*, Wiley, New Jersey, 2011

35. W.Y. Li, Study on Effect of Particle Parameters on Deposition Behavior, Microstructure Evolution and Properties in Cold Spraying. Xi'an Jiotong University, China

36. D. Rittel, G. Ravichandran, and S. Lee, Large Strain Constitutive Behavior of OFHC Copper over a Wide Range of Strain Rates Using the Shear Compression Specimen, *Mech. Mater.*, 2002, **34**(10), p 627-642

37. K. Ahn, H. Huh, and L. Park, Comparison of Dynamic Hardening Equations for Metallic Materials with the Variation of Crystalline Structures, *ICHSF2012*, 2012, p. 176-187

38. R.A. MacDonald and W.M. MacDonald, Thermodynamic Properties of fcc Metals at High Temperatures, *Phys. Rev. B*, 1981, **24**(4), p 1715-1724

39. A.C. Mitchell and W.J. Nellis, Shock Compression of Aluminum, Copper, and Tantalum, *J. Appl. Phys.*, 1981, **52**(5), p 3363-3374